Quasielastic neutron scattering study of the Ni diffusion mechanism in the intermetallic alloy NiSb

1993 J. Phys.: Condens. Matter 5 7215

(http://iopscience.iop.org/0953-8984/5/39/009)

J. Phys.: Condens. Matter 5 (1993) 7215–7230. Printed in the UK

Quasielastic neutron scattering study of the Ni diffusion mechanism in the intermetallic alloy NiSb

G Vogl†, O G Randl†‡, W Petry‡§ and J Hünecke‖

† Institut für Festkörperphysik der Universität Wien, A-1090 Wien, Austria
‡ Institut Laue–Langevin, 38 042 Grenoble, France
§ now Physikdepartment E13, TU München, D-8046 Garching, Federal Republic of Germany
‖ Institut für Metallforschung–Metallphysik, TU Berlin, D-1000 Berlin 12, Federal Republic of Germany; now Bundesanstalt für Materialforschung und -prüfung, D-1000 Berlin 45

Received 8 April 1993, in final form 23 June 1993

Abstract. Ni diffusion in the hexagonal NiSb intermetallic phase of approximately equiatomic composition is surprisingly fast, more than two orders of magnitude faster than Sb diffusion. In order to determine the atomic jump mechanism of the Ni atoms, quasielastic neutron scattering was carried out at two single crystals kept at 1040 °C, 1080 °C and 1100 °C. Jumps of the Ni atoms between regular sites (octahedral interstices of the Sb lattice) and double tetrahedral interstices (DTI) and back yield very satisfactory fits on the measured data. Such jumps had been proposed by Frohberg in order to explain the difference in tracer diffusivities parallel and vertical to the hexagonal c axis. Even with a 12% surplus of Ni atoms over Sb atoms in the alloy $Ni_{53}Sb_{47}$, about 4% vacancies remain on the regular Ni sites. Our measurements permit the exclusion of jumps just between the regular sites or just between the DTI sites.

1. Introduction

Intermetallic alloys are interesting not only because they possess promising technological features (Cahn 1989), but also because they attract the physicist's and the chemist's interest through a couple of remarkable traits brought about by the atomic orders which characterize these alloys.

A particularly interesting effect is the large difference in the diffusion velocities in the sublattices of some binary alloys. We shall deal here with a nickel–antimony alloy in the concentration range close to equiatomic composition. The relevant section of the NiSb phase diagram is shown in figure 1 (Leubolt *et al* 1986). In this alloy the Ni atoms diffuse faster by more than two orders of magnitude than the Sb atoms. Figure 2 shows an Arrhenius plot of Ni and Sb diffusivities in $Ni_{53}Sb_{47}$ from the tracer diffusion study of Hähnel, Miekeley and Wever (1986), in the following abbreviated to HMW. The alloy crystallizes in the NiAs or B8 structure shown in figure 3(a). In this structure the Sb atoms form a hexagonal close packed (HCP) lattice with a c/a ratio of 1.3 (ideal HCP: $c/a = 1.63$), $a = 3.98$ Å, $c = 5.16$ Å and the Ni atoms occupy the octahedral interstices.

In detail the situation appears to be more complicated: from measurements of the density and the lattice parameter in a series of NiSb alloys with different composition, Leubolt *et al* (1986) have concluded that even below 50 at% Ni some of the Ni atoms occupy interstitial sites of the Ni sublattice. Although surprising to the eye, these interstitial sites are probably the 'double tetrahedral interstices' (DTI) sometimes also called 'trigonal bipyramidal interstices' (Kjekshus and Pearson 1964).

0953-8984/93/397215+16$07.50

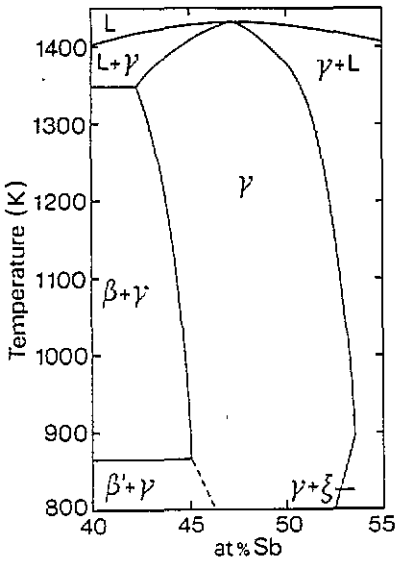

Figure 1. Phase diagram of the γ phase of NiSb according to Leubolt *et al* (1986).

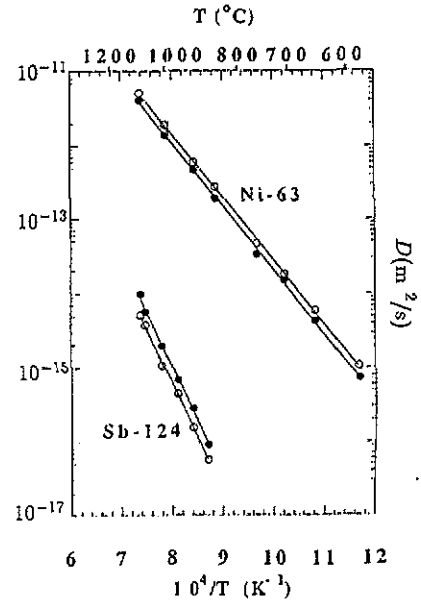

Figure 2. Arrhenius plot of ^{63}Ni and ^{124}Sb diffusion in $Ni_{53}Sb_{47}$ parallel (●) and normal (○) to the c axis according to Hähnel, Miekeley and Wever (1986).

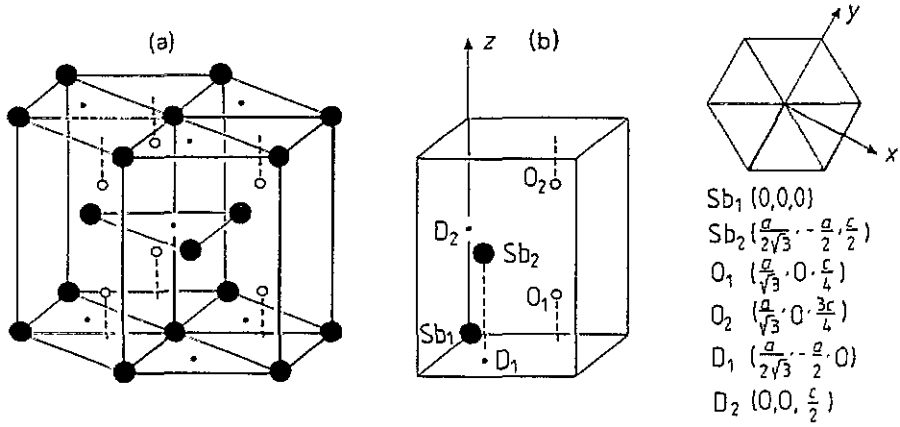

Figure 3. Structure of $Ni_{53}Sb_{47}$. Most of the Ni atoms are supposed to occupy octahedral interstitial sites (○) in the HCP lattice of the Sb atoms (●). A certain fraction, however, of the Ni atoms is supposed to occupy double tetrahedral interstices (·). (*a*) shows the HCP cell—the primitive unit cell is indicated by heavy lines; (*b*) shows the primitive unit cell with the two Sb sites and the four possible Ni sites. Also shown is the Cartesian coordinate system we used to indicate the different sites and the jump vectors of table 1. The coordinates of the sites are given as well ($a = 3.98$ Å, $c = 5.16$ Å).

The preference of the Ni atoms for interstitial sites, which leads to the creation of vacancies on the regular Ni sublattice, opens the door for a bundle of competing concepts for explaining the comparatively fast Ni diffusion. One can imagine various ways for the

Ni atoms to take advantage of the vacancies in the Ni sublattice and/or the interstitial sites:

(a) jumps exclusively via the vacant sites in the Ni sublattice;
(b) jumps almost exclusively among the interstitial sites;
(c) jumps back and forth between vacant and interstitial sites in various ways.

Only one appealing jump variant appears to be excluded, namely the jump of Ni atoms to sites in the Sb sublattice, since Sb diffusivity is 500 times slower than Ni diffusion, and it is hardly conceivable that Ni atoms could use Sb vacancies a factor of 500 times more often than the Sb atoms themselves.

In order to shed more light on the jump mechanism HMW have studied tracer diffusion in $Ni_{53}Sb_{47}$ single crystals in directions parallel and vertical to the c axis, both with ^{63}Ni and with ^{124}Sb. They found that the activation enthalpy for Ni diffusion is the same (within the error bars) vertical and parallel to the c axis (1.7 eV) and that the ratio $D_\perp/D_\parallel$ in the temperature range between 583 °C and 1083 °C is almost constant, at an average value of 1.35 ± 0.09. It is evident that this ratio first of all excludes diffusion along chains parallel to the c axis. HMW argued further that jumps exclusively between DTI sites on neighbouring planes would demand $D_\perp/D_\parallel = 0.35$ and therefore also could be excluded. A decision among other possibilities from tracer data alone is difficult. After comparing the $D_\perp/D_\parallel$ values expected from the various models with the measured value (1.35), HMW preferred a model where the Ni atom jumps from its regular site in the Ni sublattice (octahedral site of Sb sublattice) into one of the DTI sites and afterwards back to a regular site. Recently Schmidt *et al* (1992) compared HMW's results with the diffusivities in two other Ni-containing NiAs phases and concluded that this mechanism is dominating the Ni diffusion in all three alloys.

It appeared challenging for us to test these conclusions with an atomistic method which can determine the jump vector directly.

2. Investigations of elementary jump vector with an atomistic method

A comparison of potentials and limits of atomistic methods for studying diffusion, in particular of the nuclear methods, quasielastic neutron scattering (QNS), Mössbauer spectroscopy and nuclear magnetic resonance (NMR), has been given by Petry and Vogl (1987).

The principle of QNS is to measure the small broadening in energy of the 'elastically' scattered intensity that is induced by atomic movements on a time scale τ of the order of 10^{-8} seconds and shorter, corresponding to diffusivities $D \simeq \langle l^2 \rangle / 6\tau$ (with l the jump vector) of the order of 10^{-12} m^2 s^{-1} or faster. For diffusivities as slow as 10^{-12} m^2 s^{-1} (as in our case) back-scattering spectrometers or spin-echo spectrometers have to be applied. We have used the back-scattering spectrometer IN10 at the Institut Laue–Langevin (ILL) in Grenoble.

Incoherent neutron scattering probes the diffusion of a single atom, the process determining the tracer diffusion coefficient i.e. the physical property investigated by HMW (1986). For jumps in a Bravais lattice, the theory (Singwi and Sjölander 1960, Chudley and Elliot 1961, Springer 1972) yields a Lorentzian line broadening of the elastic neutron scattering intensity, as a function of the momentum transfer to the neutron scattering vector $\hbar Q$ and the energy transfer $\hbar\omega$.

$$S_{\mathrm{inc}}(Q, \omega) \propto \frac{\Gamma(Q)/2}{[\Gamma(Q)/2]^2 + (\hbar\omega)^2} \tag{1}$$

where, for the simplest case of jumps only to nearest-neighbour (NN) sites and neglecting correlations between consecutive jumps, the line width (FWHM) reads

$$\Gamma(\boldsymbol{Q}) = \frac{2\hbar}{\tau}\left[1 - \frac{1}{N}\sum_{n=1}^{N}\exp(\mathrm{i}\boldsymbol{Q}\cdot\boldsymbol{l}_n)\right]. \tag{2}$$

$\boldsymbol{l}_n$ is the nth of N jump vectors and τ the residence time of *an atom* at one lattice site between the jumps.

For jumps in a non-Bravais lattice with i sublattices the expression for the line width is considerably more complicated: Rowe *et al* (1971) have set up the rate equations for finding a diffusing atom at a point in the ith sublattice at time t. They calculated an intermediate scattering function $I(\boldsymbol{Q}, t)$ which is given by the Fourier transform of the system of rate equations. They showed that in order to determine line widths and relative intensities one has to diagonalize the jump matrix that describes jumps between inequivalent sites in one unit cell.

NiSb has four Ni sites in the hexagonal unit cell, two regular sites of octahedral symmetry and two double tetrahedral interstices (DTI sites), see figure 3(*b*). The Rowe theory is still too simple because of the unequal occupancy of the regular and the DTI sites, and an extended theory has to be used, the results of which were given first by Anderson *et al* (1984) and which have been published recently in detail by Richter *et al* (1991).

Since there are four Ni sites in the unit cell, the Ni jump matrix $\boldsymbol{A}$ is a 4×4 matrix with the elements

$$A_{ij} = \frac{1}{n_{ji}\tau_{ji}}\sum_{k}\exp(-\mathrm{i}\boldsymbol{Q}\cdot\boldsymbol{l}_{ijk}) - \delta_{ij}\sum_{j}\frac{1}{\tau_{ij}}. \tag{3}$$

Here $1/\tau_{ij}$ is the jump frequency from a site in the ith sublattice to a site in the jth sublattice, $\boldsymbol{l}_{ijk}$ is the jump vector from a site in the ith sublattice to the kth site in the jth sublattice and n_{ij} is the number of NN sites in the jth sublattice to an atom in the ith sublattice. For NN jumps the n_{ij} are all equal, namely $n_{ij} = 6$, since there are six Ni NN of octahedral geometry for any DTI Ni atom and vice versa.

The scattering law is made up of four Lorentzians, the widths of which (HWHM) are the eigenvalues of the matrix $\boldsymbol{A}$, the weighting factors w_p being given by the eigenvectors:

$$S_{\mathrm{inc}}(\boldsymbol{Q}, \omega) = \sum_{p}\frac{w_p(\boldsymbol{Q})\Gamma_p(\boldsymbol{Q})/2}{[\Gamma_p(\boldsymbol{Q})/2]^2 + (\hbar\omega)^2}. \tag{4}$$

Measurements of the line widths as a function of momentum transfer contain information about the jump vectors $\boldsymbol{l}$. $\boldsymbol{l}$ can be deduced from the dependence of Γ_p on $\boldsymbol{Q}$, whereas the residence times τ_{ij} (jump frequency $1/\tau$) can be obtained from the absolute values of the line widths at a given temperature. In other words: information is derived by comparing shapes and sizes of $\Gamma_p(\boldsymbol{Q}, T)$ with model predictions. Since it is easily possible that several models would produce a more or less identical dependence of Γ_p on $\boldsymbol{Q}$ for *one* sample orientation, one performs a couple of measurements changing the sample orientation, that is to say the scalar product $\boldsymbol{Q}\cdot\boldsymbol{l}$. Measurements with appropriately chosen sample orientations will allow discrimination between the different models. Recently, Vogl *et al* (1989) successfully performed such measurements and determined the elementary jump vector in β-titanium. To our knowledge the present work is the first to determine the elementary jump vector in an *intermetallic phase* by means of QNS.

Naturally no method is without restriction. In the case of QNS restrictions become distinct if one leaves the well-paved path of hydrogen diffusion. It has already been mentioned that diffusivities of at least 10^{-12} m^2 s^{-1} are nowadays necessary (spin-echo will lower that limit). For atoms other than hydrogen, diffusivities of this order are only realized close to the melting point.

A second condition consists in the need of a sufficiently high incoherent scattering cross section. No isotope can compete here with hydrogen (σ_{inc} = 80 barn), but nickel is not bad: for Ni σ_{inc} = 5.2 barn. The incoherent scattering cross section of Sb is only 0.3 barn (Sears 1984), therefore practically all the incoherent scattering from NiSb comes from Ni, and Sb is invisible for QNS.

Coherent scattering which is unavoidable for most elements turns out to give rise to additional problems: this kind of scattering probes the pair correlation, i.e. the correlated motion of diffusing atoms, instead of the self-correlation probed by incoherent scattering. Ross and Wilson (1978) and Sinha and Ross (1988) have discussed the interesting aspects of measuring coherent quasielastic scattering which allows information to be obtained on the interaction of atoms of the diffusing species. However, only very few experiments have been carried out and, of course, again in the field of hydrogen (the isotope deuterium has a reasonably coherent cross section) which diffuses sufficiently quickly and therefore lends itself to time-of-flight measurements profiting from much higher intensities than our back-scattering measurements. Deconvolution of the quasielastic curves into incoherent and coherent parts (Hempelmann *et al* 1988) and a most sophisticated separation of coherent and incoherent scattering by help of spin-flip analysis of polarized neutrons (Cook *et al* 1990) give first indication of the direction to follow.

In the present case the situation of coherent scattering appears to be as follows: since, as has been reported in section 1, the diffusivity of the Sb atoms is much lower than that of the Ni atoms, jumps of Ni atoms to sites on the Sb sublattice can be excluded. Therefore, the defects on the Sb sublattice, because of their low concentration, will give a negligible contribution to coherent scattering compared to defects on the Ni sublattice. The rather fast diffusion of Ni must then be caused by disorder on the Ni sublattices, i.e. the regular Ni sublattice and the DTI sublattice. We shall attempt to estimate the corresponding contribution of coherent scattering for one special model in section 5.

3. Samples used

The single crystal samples of $Ni_{53}Sb_{47}$ had been grown by the Bridgman technique in the same way as the crystals used for the HMW tracer experiments. $Ni_{52.7}Sb_{47.3}$ (and *not* $Ni_{50}Sb_{50}$) is exactly the composition with maximum melting point of the γ phase (figure 1).

We have cut our two single crystals into slices of two different orientations and thickness of 4 mm using a low-speed diamond saw. The slices were ground in order to make them completely flat and smooth. Finally, their surface was etched with a mixture of HNO_3 and H_2SO_4. The slices were fitted together in order to reach an effective sample surface of 30 × 30 mm^2. Sample 1 was composed of two pieces with the c axis lying in their surface. Sample 2 consisted of four parallely oriented parts with their large surfaces perpendicular to the c axis. Then the samples were fitted into the holders made of Nb. Laue x-ray photographs confirmed the excellent correspondence of all pieces concerning crystal orientation.

In some preparatory experiments we found that we had to exclude any contact between sample and holder in order to prevent the formation of a niobium-NiSb eutecticum. Such a

eutecticum is unavoidably formed at the measuring temperatures (about 1100 °C) if there is contact, and leads to melting and destruction of sample, sample holder and container within a short time. To prevent direct contact we clamped thin strips of oxide ceramics between Nb sample holder and sample. These diffusion barriers proved to be absolutely necessary; their loss (occurring twice following experimental mistakes) led immediately to melting and loss of the sample. Figure 4 shows the sample and sample holder for sample 1.

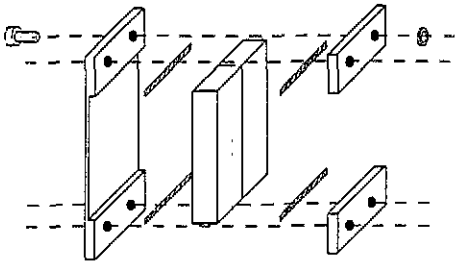

Figure 4. Sample and holder for sample 1. Ceramic strips (shaded) had to be clamped between the Nb sample holder and the specimen in order to prevent diffusion between one another.

Finally, each sample holder was welded into a vacuum-tight thin-walled Nb container in order to prevent decomposition via Sb loss at the measuring temperatures where the Sb vapour pressure reaches high values.

4. Experiments and evaluation of data

An ILL furnace with a number of heat shields to guarantee temperature homogeneity and stability and with a tube-like resistor heater made of Nb has been used. The furnace maintained the Nb can containing the specimen at the measuring temperatures with an estimated absolute error of ± 10 °C (relative error between subsequent measuring temperatures was considerably smaller). Different crystal orientations were obtained by turning the whole furnace on the goniometer of IN10.

For each crystal orientation a measurement took $1\frac{1}{2}$ days on average. The neutrons which had been scattered from the specimen in different directions and were subsequently back-scattered from the analyser crystals of IN10 were detected simultaneously by eight detectors. For a wavelength of the incoming neutrons of 6.275 Å the analyser positions corresponded to momentum transfers Q between 0.27 $Å^{-1}$ and 1.95 $Å^{-1}$. The principles of registering quasielastic energy distribution with IN10 may be found in the pioneering paper by Alefeld, Birr and Heidemann (1969) or in a recent paper by Alefeld *et al* (1992).

We took four measurements at 1080 °C and one at 1040 °C with sample 1 and two measurements at 1100 °C with sample 2. The corresponding orientations of the crystals are explained in figure 5. Figure 6 shows a typical spectrum. In addition we performed some 'empty can' measurements, that is to say, measurements of can and holder without sample in order to be able to separate the scattering by the can from the scattering by the sample. Finally the effective resolution of the instrument was determined with the sample in the different orientations but at room temperature, thus avoiding quasielastic broadening.

The data were processed in the following way by the programme SQW available at ILL (Anderson and Nelson 1985): The empty-can data were subtracted from the specimen data. Subsequently the scattering function $S(Q, \omega)$ was calculated from the reduced data taking into account the resolution measurements. Absorption effects were corrected for by considering the geometry for each orientation. The so-prepared data were fitted with

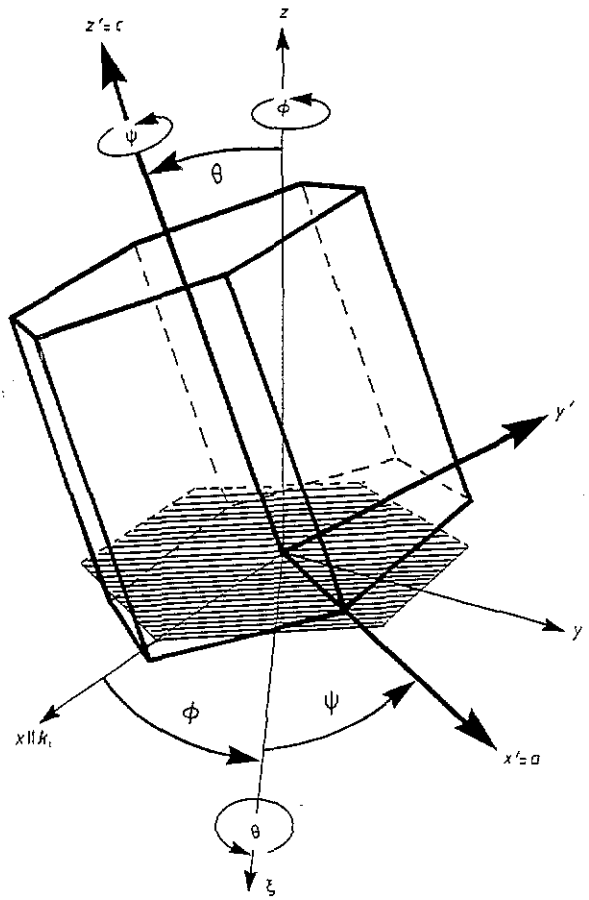

Figure 5. Scheme of the crystal orientation with respect to the laboratory frame x, y, z as defined by the back-scattering spectrometer IN10. The incident neutron wave vector k_i is parallel to the x axis, and the scattered wave vector k_f varies in the xy plane according to the analyser positions. The orientation of a crystal, symbolized in the figure by a hexagonal prism with a axis and c axis, is described by the three Euler angles (Φ, Θ, Ψ) as defined by Goldstein (1980). These angles describe rotations which turn the crystal from the laboratory frame x, y, z (where the a axis is parallel to the x axis and the c axis is parallel to the z axis, the base plane of the hexagonal prism in the x, y, z frame being shown shaded) into the crystal frame x', y', z'. In order to reach the position (Φ, Θ, Ψ) one first turns around z by Φ degrees, then around the next x axis ξ by Θ degrees and finally around z' by Ψ degrees. All rotations are anticlockwise as indicated by the arrows. The Euler angles (in degrees) for our measurements were (30, 90, 90) for the measurement at 1040 °C, (−30, 90, 90), (0, 90, 90), (30, 90, 90), (60, 90, 90) at 1080 °C and (90, 90, 45), (60, 90, 45) at 1100 °C.

Lorentzian lines using routine ILLFIT adapted to these problems by R Hempelmann and his colleagues at the KFA Jülich. Finally corrections for multiple scattering were applied by using the programme DISCUS (Johnson 1974). Two-line fits were performed with the routine WLL at ILL.

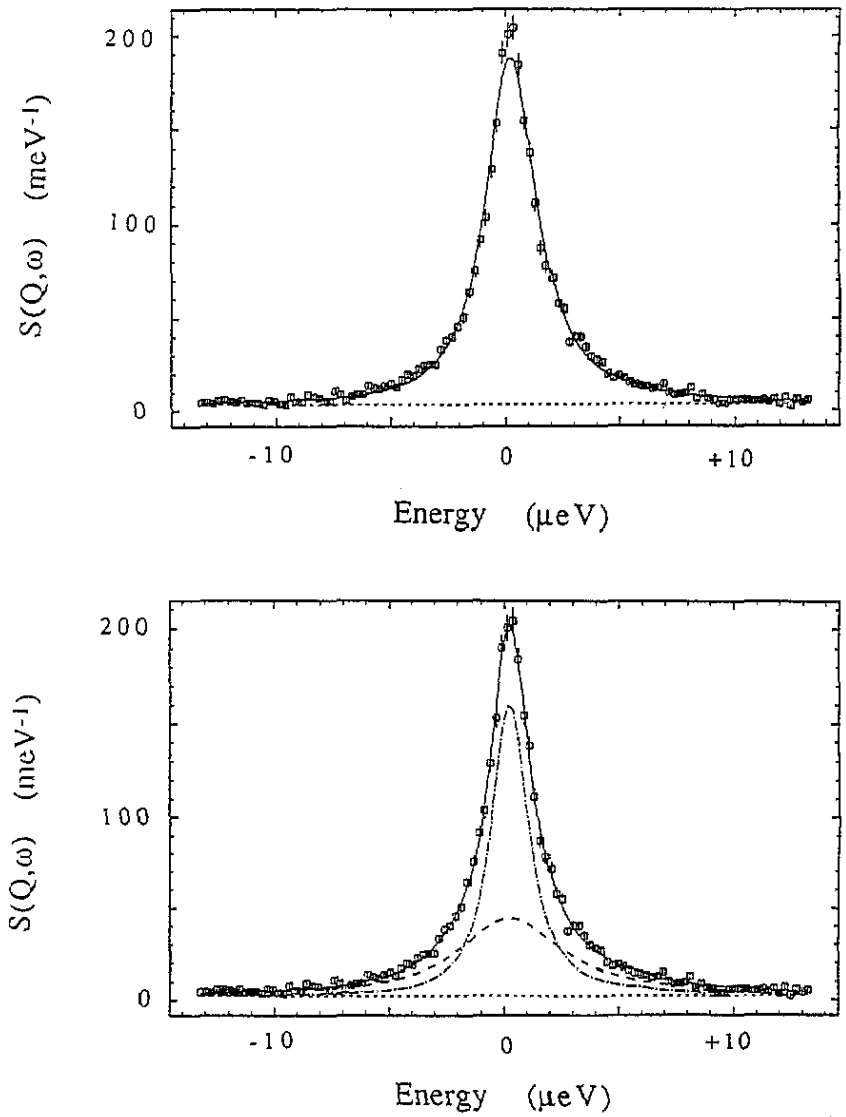

Figure 6. Typical QNS spectrum for crystal orientation (90, 90, 45) and $Q = 1.92$ Å^{-1}, taken at 1100 °C. Note that a fit with just one Lorentzian (top figure) is worse than a two-Lorentzian fit (bottom figure).

5. Models for the elementary jump process

Measurements by the tracer diffusion method register the net result of a great number of single-atom diffusion jumps. Methods like QNS which study diffusion on an atomistic scale possess the advantage over the tracer diffusion method that they are more capable of distinguishing between the details of different models. This becomes evident in our case: HMW measured the ratio $D_\perp/D_\parallel$. By comparing the experimental value with predictions from two models: ((a) jumps between DTI sites and (b) back-and-forth jumps between regular and DTI sites) they were able to exclude model (a). Tracer studies, however, are not selective enough to decide between models which differ, e.g. only in the percentage of the

Ni atoms at any moment on DTI sites. We shall show that QNS can make such a decision.

5.1. Jumps between regular lattice sites in the Ni sublattice

Thinking in analogies one might as a first choice propose jumps of the Ni atoms via vacant sites in the regular Ni sublattice, i.e. the sublattice made up by the octahedral interstices of the Sb lattice, analogous to the jumps via vacancies prevailing in metallic lattices. This model, however, is irreconcilable not only with the HMW tracer results but also with our QNS results as will be shown in the following.

The octahedral Ni sites form a hexagonal Bravais lattice and, therefore, jumps in this lattice should be described in the frame of the Chudley-Elliott (1961) theory. At a closer look it turns out that there are three possible jumps to neighbouring sites:

(1) the nearest neighbours of each Ni atom are situated at a distance of $\pm c/2$ parallel to the c axis. Diffusion caused exclusively by that mechanism along chains would not show any component normal to the c axis ($D_\perp/D_\parallel$=0), which is in contradiction to HMW's results.

(2) The octahedral sites in the basal plane are more distant (distance a) and again cannot be the only path of diffusion since there is no component parallel to the c axis ($D_\perp/D_\parallel = \infty$).

(3) Finally, there are octahedral neighbours diagonally above and below each octahedral site (distance $\sqrt{(a^2+c^2)/4}$). The situation is outlined in figure 7(a).

Indeed, a mixture of these three mechanisms might be reconcilable with the tracer data. In order to calculate the resulting line width one has to determine the width that each of the three mechanisms would produce on its own, and sum up the widths obtained by weighting them corresponding to the relative probability of the mechanism. Thus, a single Lorentzian line has to be expected. Figure 8(a) shows the corresponding line widths of all our spectra and figure 8(b) the expected Q dependence. For the crystal orientation that corresponds to $\Phi = -30°$, $\Theta = 90°$, $\Psi = 90°$ (for definition of the Euler angles see figure 5) all three theories for jumps between regular Ni sites show a distinct minimum, thus any mixture would have a minimum too. That minimum, however, has no equivalent in our data. A comparison with figure 8(a) shows that also for other crystal orientations the expected Q dependences are far from being realistic.

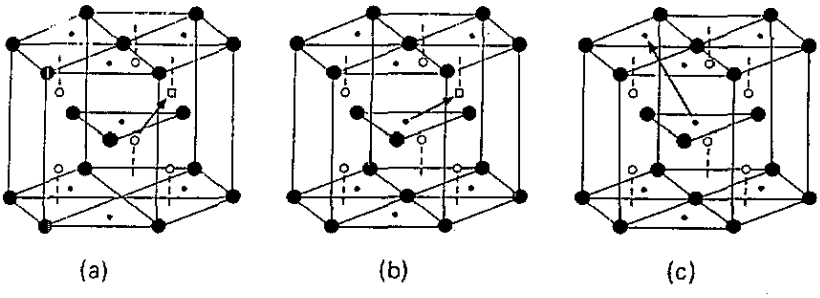

Figure 7. Exemplary jump vectors for each of the three models discussed in the text. Symbols are the same as in figure 3. In model (a) the Ni atoms jump between their regular sites, i.e. the octahedral interstices in the HCP Sb sublattice. According to the Frohberg model (b) the Ni atoms jump alternately between the regular sites and the double tetrahedral interstices (DTI). The DTI model (c) assumes jumps exclusively between the DTI sites.

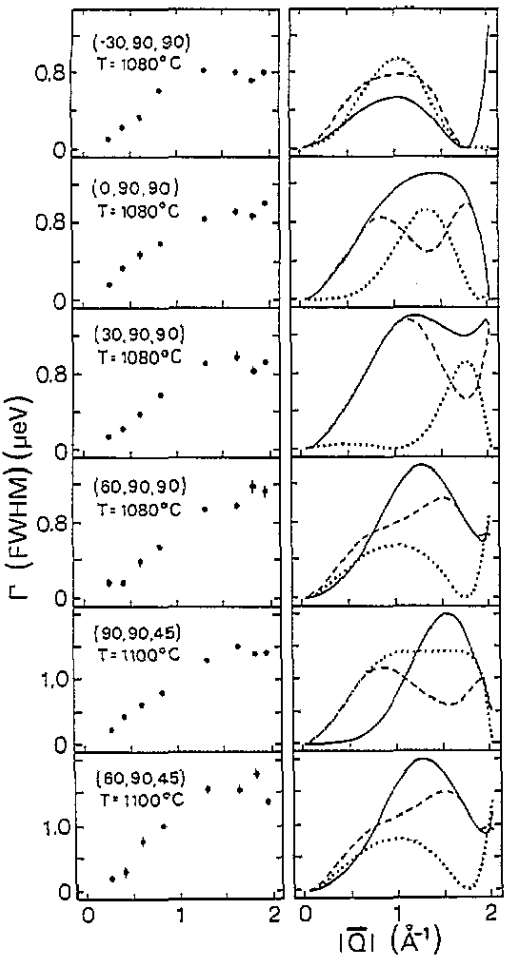

Figure 8. Results of measurements and fits with just one Lorentzian (left column) with the crystal orientations defined by the Euler angles (Φ, Θ, Ψ), in comparison to the predictions (right column) of the line width for jumps between the regular 'octahedral' sites (solid line: chain jumps parallel to the c axis; dotted line: jumps in the plane normal to c; dashed line: diagonal jumps).

5.2. Jumps between regular and DTI sites

In order to explain the preponderance of the diffusion normal to the c axis, HMW, following a suggestion by Frohberg, proposed the jump mechanism as sketched in figure 7(*b*). We shall call these jumps 'Frohberg jumps', and they can be imagined as follows: a Ni atom leaves its regular lattice site (octahedral site of the Sb lattice), jumps to a DTI, but then cannot continue jumping in the DTI sublattice but rather uses the next opportunity to jump back into an octahedral lattice site. Of course, for a jump to be effective for diffusion, that site cannot be the original site from where the jumping atom has started, but the vacancy must be filled up by another Ni atom having started from another DTI. The model predicts $D_\perp/D_\parallel = 8a^2/3c^2 = 1.57$, which is not too different from the experimental result of 1.35 ± 0.09.

These jumps take place in a non-Bravais lattice. As can be seen from figure 3 there are four sublattices, i.e. four sites of different local symmetry in the unit cell: two regular sites of octahedral geometry (O_1, O_2) and two of the DTI type (D_1, D_2). We assume that the jump frequency for jumps from an octahedral site to a DTI site is the same for all possible combinations:

$$\frac{1}{\tau_{O_1D_1}} = \frac{1}{\tau_{O_1D_2}} = \frac{1}{\tau_{O_2D_1}} = \frac{1}{\tau_{O_2D_2}} =: \frac{1}{\tau_1} \tag{5}$$

and that the same holds true for the jumps back:

$$\frac{1}{\tau_{D_1O_1}} = \frac{1}{\tau_{D_1O_2}} = \frac{1}{\tau_{D_2O_1}} = \frac{1}{\tau_{D_2O_2}} =: \frac{1}{\tau_2}. \tag{6}$$

The two jump frequencies $1/\tau_1$ and $1/\tau_2$ are not independent: detailed balance between the sublattices demands that

$$c_O/c_D = \tau_1/\tau_2 =: \alpha. \tag{7}$$

Here c_O and c_D are the concentrations of Ni atoms in the octahedral (regular) and DTI sublattices, respectively. The set of jump vectors l_{ijk} is given in table 1.

Table 1. Set of jump vectors necessary to construct A for jumps between octahedral and DTI sites. All redundant vectors have been left out: to obtain for example, the set $l_{D_1O_1}$ corresponding to $D_1 \rightarrow O_1$ jumps, one has to take the vectors $l_{O_1D_1}$ and change their sign. The coordinates are the same as in figure 3. a and c are the lattice parameters of the HCP lattice: $a = 3.98$ Å, $c = 5.16$ Å.

$O_1 \rightarrow D_1$: $l_{O_1D_1}$	$\left(-\frac{a}{2\sqrt{3}}, -\frac{a}{2}, -\frac{c}{4}\right)$	$\left(\frac{a}{\sqrt{3}}, 0, -\frac{c}{4}\right)$	$\left(-\frac{a}{2\sqrt{3}}, \frac{a}{2}, -\frac{c}{4}\right)$
$O_1 \rightarrow D_2$: $l_{O_1D_2}$	$\left(\frac{a}{2\sqrt{3}}, \frac{a}{2}, \frac{c}{4}\right)$	$\left(-\frac{a}{\sqrt{3}}, 0, \frac{c}{4}\right)$	$\left(\frac{a}{2\sqrt{3}}, -\frac{a}{2}, \frac{c}{4}\right)$
$O_2 \rightarrow D_1$: $l_{O_2D_1}$	$\left(-\frac{a}{2\sqrt{3}}, -\frac{a}{2}, \frac{c}{4}\right)$	$\left(\frac{a}{\sqrt{3}}, 0, \frac{c}{4}\right)$	$\left(-\frac{a}{2\sqrt{3}}, \frac{a}{2}, \frac{c}{4}\right)$
$O_2 \rightarrow D_2$: $l_{O_2D_2}$	$\left(\frac{a}{2\sqrt{3}}, \frac{a}{2}, -\frac{c}{4}\right)$	$\left(-\frac{a}{\sqrt{3}}, 0, -\frac{c}{4}\right)$	$\left(\frac{a}{2\sqrt{3}}, -\frac{a}{2}, -\frac{c}{4}\right)$

In order to compare the model predictions with the experimental results we have calculated the eigenvalues of the 'jump matrix' A (3) and the corresponding weights for all crystal orientations of the experiment and for a wide range of ratios $\alpha = \tau_1/\tau_2$. Figure 9(a) to (c) show the results of the calculations, i.e. expected eigenvalues and weights of the four quasielastic lines, by way of examples, namely for the crystal orientation (−30, 90, 90) and for three different ratios α, $\alpha = 9$, $\alpha = 5$ and $\alpha = 1$.

The following items are worth noting:

(i) As $Q \rightarrow 0$, only one eigenvalue which is proportional Q^2, contributes to S_{inc}, the weights of all other lines being zero. Thus, at small Q, one obtains a single Lorentzian with width proportional to Q^2, in agreement with the results of the diffusion theory.

(ii) In view of the rather limited experimental resolution it is fortunate that for realistic values of α a fit with two lines, instead of four lines, should be sufficient since in all cases one of the narrower lines has practically no intensity and/or the expected widths of the broad lines are not very different. We therefore decided to use a fitting procedure with only two Lorentzians, a narrow line with width Γ_n and a broad one with width Γ_b.

(iii) The ratio of the widths of the narrow line at its first maximum ($Q = 1.2$ Å), and that of the two broad lines scales with α.

(iv) For the crystal orientation of figure 9, (−30, 90, 90), the width of the narrowest line (corresponding to the smallest eigenvalue at $Q = 0$), after increasing at low Q up to $Q = 1$ Å^{-1}, should decay down to zero value at $Q = 1.75$ Å^{-1}. Other crystal orientations show similar characteristic features.

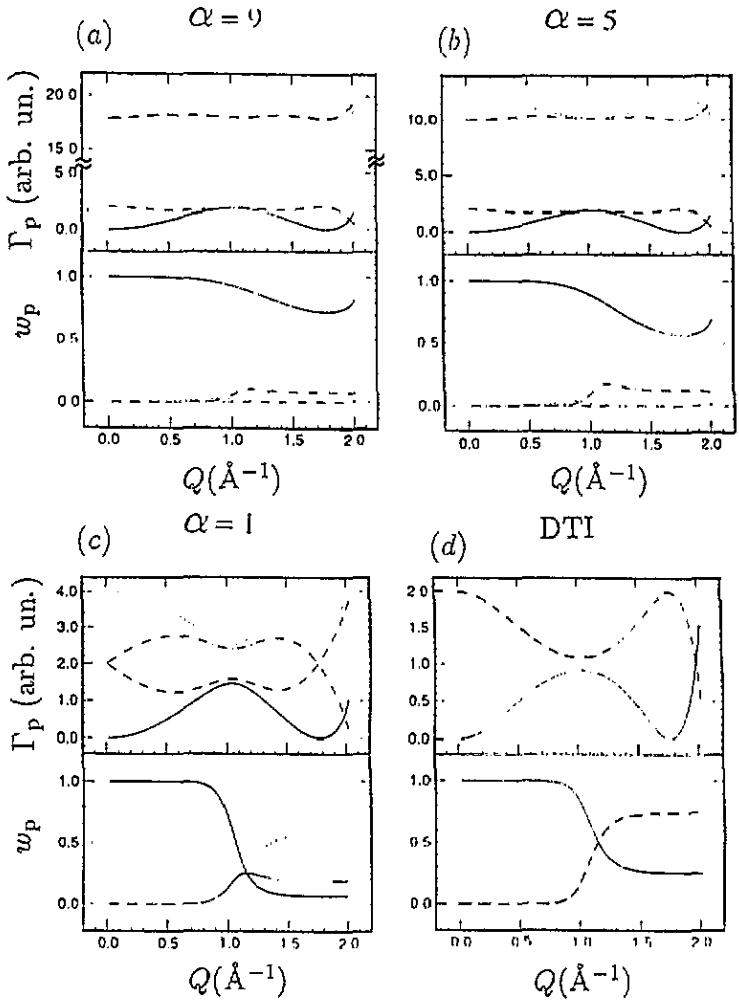

Figure 9. Crystal orientation (−30, 90, 90). Eigenvalues Γ_p (upper row) and weights w_p (lower row) for jumps between regular and DTI sites and three different values of $\alpha = c_O/c_D$ ((*a*) to (*c*)) and for jumps exclusively via DTI sites (*d*).

We decided to use the following procedure in order to decide which parameters fit best the experimental results: for each jump ratio α the weights of the two relevant eigenvalues were calculated. Then two Lorentzians were fitted to the data by keeping the relative weights fixed. The resulting line widths allowed us to examine which ratio α fitted best the experimental results, considering the following conditions:

(i) the transition from the region with only one Lorentzian ($Q < 1$) to that with two Lorentzians had to be continuous,

(ii) at a Q value of 1.2 Å^{-1} the ratio R of the widths of broad and narrow line had to coincide with α,

(iii) the Q dependence of the width of the narrow line had to agree with that given by the theory.

Figure 10 shows in its upper row the Q dependence as predicted by O↔DTI models with different jump ratios α. In the lower row the experimental data for (−30, 90, 90) are

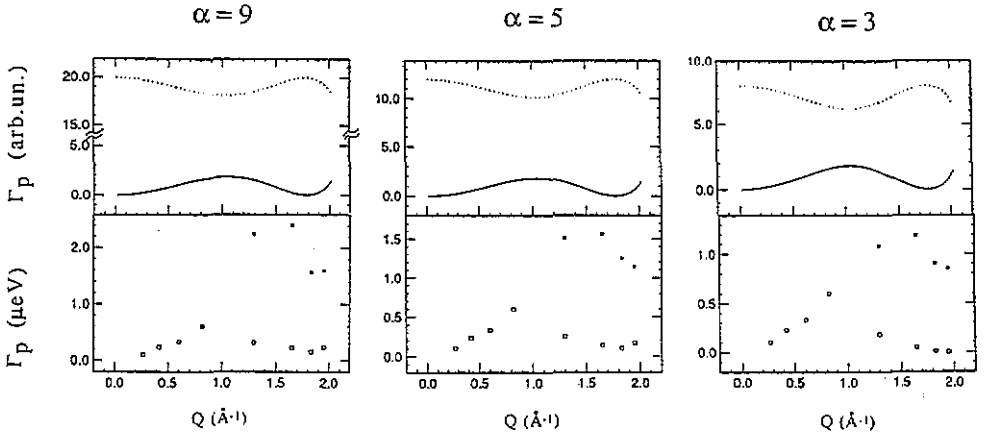

Figure 10. Crystal orientation (−30, 90, 90). Comparison of Q dependence of eigenvalues predicted by model of jumps between regular and DTI sites, reduced to two averaged eigenvalues (upper row), and line widths recieved from fits with two Lorentzians, a broad and a narrow one (lower row).

shown. It is evident that the Q dependence of the line width of the narrow line follows the model: a minimum in the range between $\alpha = 3$ and 9. At α values lower than 3 or higher than 9 there is no longer a similarity of experimental and theoretical curves.

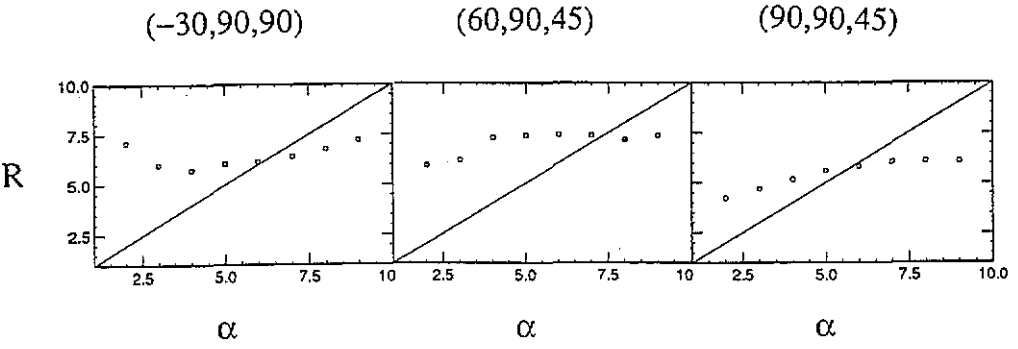

Figure 11. Ratio R of widths of broad and narrow lines Γ_b/Γ_n at $Q = 1.2$ Å^{-1} for three crystal orientations. Note that R comes closest to the expected model value of α at values between 5 and 7.

Figure 11 shows by way of three crystal orientations that optimum agreement of the ratio $R = (\Gamma_b/\Gamma_n)$ at $Q = 1.2$ Å^{-1} with the expected values is attained for α between 5 and 7, though for some orientations no conclusion was possible.

From α we can conclude on the fractions of Ni atoms at any moment on octahedral and on DTI sites, respectively (compare (7)). With $\alpha = 6 \pm 2$ we receive an occupation ratio $c_D/c_O = (0.14^{+0.06}_{-0.03})$. For the alloy $Ni_{53}Sb_{47}$, for which 53% of all atoms are Ni atoms, this corresponds to an occupation of 16% of the DTI sites. This is different from what has often been assumed, i.e. practically 100% occupation of octahedral sites and only the surplus

atoms on DTI sites (i.e. 12% for $Ni_{53}Sb_{47}$). Our results indicate a non-negligible vacancy concentration on octahedral sites of about 4%, even for a Ni surplus in the alloy.

In the following we consider a possible contribution from coherent scattering. For Bravais lattices Ross and Wilson (1978) have found that the coherent scattering function $S_{coh}(Q, \omega, c)$, for diffusion on a lattice with a fraction c of occupied sites, is connected in the following way with the incoherent scattering function S_{inc}:

$$S_{coh}(Q, \omega, c) = c(1-c)S_{inc}(Q, \omega, 0) \tag{8}$$

with $S_{inc}(Q, \omega, 0)$ the incoherent scattering function for diffusion on an empty lattice ($c = 0$). For diffusion via vacancies this implies that the width Γ_{coh} of the coherent quasielastic line may be much larger than that of the incoherent line, since the width of the former scales with $1/\tau(0)$, whereas the width of the latter scales with $1/\tau(c)$. Here $\tau(0)$ and $\tau(c)$ are the residence times for jumps on an empty lattice and on a lattice with a fraction c of occupied sites, respectively.

For non-Bravais lattices with more than one quasielastic line, to our knowledge there has been no attempt to calculate coherent scattering, and it is not evident how one has to proceed to calculate S_{coh} for jumps between the regular and the interstitial lattice. We may, however, assume that the intensities of the coherent lines again scale with $c(1-c)$, where c is the occupation of the regular and the DTI lattice, respectively. This implies that intensities of the coherent lines are lower than the intensities of the incoherent lines. We may further assume that the coherent lines are considerably broader than the incoherent lines. We then deduce that, even though the coherent intensities scale with the rather high coherent scattering cross section of nickel, they are small and the line widths are as large as to be hardly detectable above the background.

The best chance of finding the coherent contributions would be at low Q where one coherent line (presumably the narrowest line would again have 100% weight) could still be narrow enough not to be lost in the background. However, we were unable to find any indication for such a line and therefore have to deduce that the coherent contribution even there is too broad and too small to be detectable.

5.3. *Jumps exclusively via DTI sites*

We have tested whether jumps exclusively via DTI sites (figure 7(*c*)) would be a possibility. The DTI lattice is a compressed HCP lattice, i.e. it contains two atoms per unit cell. The corresponding jump matrix is a 2×2 matrix, its eigenvalues and the corresponding weights are given in figure 9(*d*) for $(-30, 90, 90)$. It is clear that the model is in contrast to the experimental data for that direction, since there should be essentially only one narrow Lorentzian at about 1.00 $Å^{-1}$ ($R \simeq 1$). Similar discrepancies appear for other directions.

This is in agreement with HMW's conclusions: they also excluded this model since it predicts $D_\perp/D_\parallel = 0.39$ in striking contrast to their measurements $D_\perp/D_\parallel = 1.35 \pm 0.09$.

5.4. *Diffusivity*

The line width at small Q is connected to the diffusivity D through (see e.g. Singwi and Sjölander 1960)

$$\lim(Q \to 0)\Gamma = 2\hbar D Q^2. \tag{9}$$

The macroscopic diffusivity can therefore be derived from the Q dependence of the line width at small Q. Here for all models one Lorentzian line prevails. From the experimental results at 1040 °C, 1080 °C and 1100 °C we obtain

$$D(1040\,^{\circ}\mathrm{C}) = 5 \times 10^{-12}\ \mathrm{m^2\ s^{-1}},$$
$$D(1080\,^{\circ}\mathrm{C}) = 8 \times 10^{-12}\ \mathrm{m^2\ s^{-1}}\ \text{(averaged)}$$
$$D(1100\,^{\circ}\mathrm{C}) = 16 \times 10^{-12}\ \mathrm{m^2\ s^{-1}}\ \text{(averaged)}.$$

Remember that the $\Gamma(Q)$ values of figures 8 and 10 have undergone multiple scattering corrections and at low Q are particularly dependent on the corrections.

Evidently the agreement with the tracer data (figure 2) is not particularly satisfactory, but it is within error bars. It should be stressed here that the atomistic methods (QNS, Mössbauer, NMR) do not provide a better way to determine macroscopic diffusivities. In that field the accuracy of tracer diffusion measurements is highly superior. The virtue of the atomistic methods lies rather in their ability to probe the elementary diffusion event. For a discussion of this point see Petry and Vogl (1987).

6. Conclusion

Among the various models which are conceivable for explaining the surprisingly fast Ni diffusion in the intermetallics $Ni_{53}Sb_{47}$, best agreement with the measured QNS data is for jumps from regular (octahedral) sites to double tetrahedral interstitial sites and vice versa (Frohberg jumps), whereas jumps between interstitial sites only or via vacancies from regular site to regular site can certainly be excluded.

Acknowledgments

The idea for this work arose in discussions with H Wever and members of his institute at the TU, Berlin. He and his collaborators also provided the crystals, thus to them we owe our best thanks. One of us (OGR) thanks R Hempelmann for introducing him to the programmes ILLFIT and DISCUS and K Schroeder for discussions. We thank B Sepiol for help with the theory and K W Kehr for valuable discussions on the problems of correlation effects.

This work was financed by the Austrian Fonds zur Förderung der Wissenschaftlichen Forschung (FWF), contracts P7426 and S5601.

References

Alefeld B, Birr M and Heidemann A 1969 *Naturwissenschaften* **56** 410

Alefeld B, Springer T and Heidemann A 1992 *Nucl. Sci. Eng.* **110** 84

Anderson I and Nelson R 1985 *Institut Laue–Langevin Report* 85AN8T

Anderson I S, Heidemann A, Bonnet J E, Ross D K, Wilson S K and McKergow M 1984 *J. Less-Common Met.* **101** 405

Cahn R W 1989 *Metals, Mater. Proc.* **1** 1

Chudley C T and Elliott R J 1961 *Proc. Phys. Soc.* **77** 353

Cook J C, Richter D, Schärpf O, Benham M J, Ross D K, Hempelmann R, Anderson I S and Sinha S K 1990 *J. Phys.: Condens. Matter* **2** 79

Goldstein H 1980 *Classical Mechanics* 2nd edn (Reading, MA: Addison-Wesley)
Hähnel R, Miekeley W and Wever H 1986 *Phys. Status Solidi* a **97** 181
Hempelmann R, Richter D, Faux D A and Ross D K 1988 *Z. Phys. Chem. NF* **159** 175
Johnson M W 1974 *AERE Harwell Report* R7682
Kjekshus A and Pearson W B 1964 *Progress in Solid State Chemistry* vol 1, ed H Reiss (Oxford: Pergamon) p 83
Leubolt R, Ipser H, Terzieff P and Komarek K L 1986 *Z. Anorg. Allg. Chem.* **533** 205
Petry W and Vogl G 1987 *Mater. Sci. Forum* **15–18** 323
Richter D, Hempelmann R and Schönfeld C 1991 *J. Less-Common Met.* **172–174** 595
Ross D K and Wilson D L T 1978 *Neutron Inelastic Scattering* vol 2 (Vienna: IAEA) p 383
Rowe J W, Sköld K, Flotow H E and Rush J J 1971 *J. Phys. Chem. Solids* **32** 41
Schmidt H, Frohberg G and Wever H 1992 *Acta Metall. Mater.* **40** 3105
Sears V F 1984 *Chalk River Nuclear Laboratories Report* AECL-8490
Singwi K S and Sjölander A 1960 *Phys. Rev.* **119** 863
Sinha S K and Ross D K 1988 *Physica* B **149** 51
Springer T 1972 *Quasielastic Neutron Scattering for the Investigation of Diffusive Motions in Solids and Liquids (Springer Tracts in Modern Physics 64)* (Berlin: Springer)
Vogl G, Petry W, Flottmann T and Heiming A 1989 *Phys. Rev.* B **39** 5025